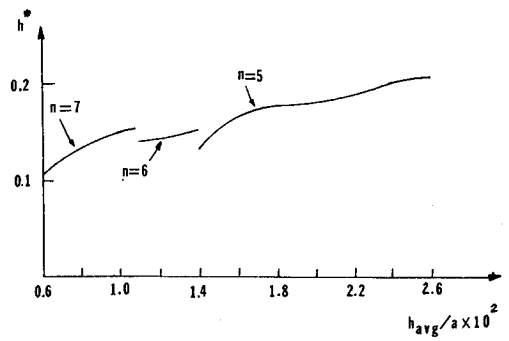

Fig. 3 Optimum thickness at the ends. $L/a = 2.0$.

to be solved for the buckling pressure, the buckling mode, and the thickness variation of the shell.

III. Results

Equations (6) were solved on an IBM 360/50 computer. For most cases, a value of $K = 15$, corresponding to eight terms in each of Eqs. (5), was sufficient to achieve convergence.

The gains achieved by optimization are shown in Fig. 2. The results show that considerable increases in the buckling pressure can be gained by varying the wall thickness. The numbers above (below) the curves in Fig. 2 refer to the number of circumferential waves in the critical mode for the optimum (constant thickness) shell. A comparison was made between the constant thickness (Batdorf) solution used here and a more exact solution.[8] For $L/a = 10.0$, it was found that the Batdorf (short shell) theory is in error by only a few percent even for a shell of this length. Figure 3 is a typical plot of the thickness at the ends versus the average thickness for $L/a = 2.0$. At the points of discontinuity of the curve, there are two geometries which yield the same buckling pressure. Each of these configurations correspond to a different number of circumferential waves in the buckled shell.

As a further result of optimization, a redistribution of buckling displacements takes place, with the maximum lateral displacement occurring between $x = 0$ and $x = L/2$.

An independent check on the validity of this method was made by disregarding the last of Eqs. (6) and using the remaining $3(K + 1)/2$ equations to generate h^* vs p_{cr} curves for a selected number of shell geometries. In all cases, the optimum found in examining these curves agreed with the optimum found directly by the procedure presented here.

References

[1] Tadjabakhsh, T. and Keller, J. B., "Strongest Columns and Isoperimetric Inequalities for Eigenvalues," *Journal of Applied Mechanics*, Vol. 29, No. 1, March 1962, pp. 159–164.

[2] Taylor, J. E., "The Strongest Column: An Energy Approach," *Journal of Applied Mechanics*, Vol. 34, No. 2, June 1967, pp. 486–487.

[3] Huang, N. C. and Sheu, C. Y., "Optimal Design of an Elastic Column of Thin-Walled Cross Section," *Journal of Applied Mechanics*, Vol. 35, No. 2, June 1968, pp. 285–288.

[4] Wu, C. H., "The Strongest Arch—A Perturbation Solution," *Journal of Applied Mechanics*, Vol. 35, No. 3, Sept. 1968, pp. 476–480.

[5] Wang, C., *Applied Elasticity*, McGraw-Hill, New York, 1953, pp. 267–271.

[6] Reynolds, T. E., "Elastic Labor Buckling of Ring-Supported Cylindrical Shells under Hydrostatic Pressure," Rept. 1614, Sept. 1962, David Taylor Model Basin.

[7] Batdorf, S. B., "A Simplified Method of Elastic Stability Analysis for Thin Cylindrical Shells," Rept. 874, 1947, NACA.

[8] Timoshenko, S. P. and Gere, J. M., "Theory of Elastic Stability," 2nd ed., McGraw-Hill, New York, 1961.

Interpretation of *n*-Dimensional Covariance Matrices

I. A. Gura* and R. H. Gersten†
The Aerospace Corporation, El Segundo, Calif.

Although error analyses constitute one of the more frequently encountered types of engineering problems, the topic is fraught with fallacies, misconceptions, and distortions. One basic difficulty occurs in attempting to interpret covariance matrices. While the usual assumption of Gaussianness is reasonable, there is a widespread tendency to assign erroneous probability confidence levels to the associated error ellipsoids. In this Note, an attempt will be made to clarify this situation.

Let x be an n-dimensional Gaussian random vector with mean $\bar{x}$ and covariance matrix C. As is well known, the probability density function for x is

$$\rho(x) = \frac{1}{(2\pi)^{n/2}(\det C)^{1/2}} \exp\left[-\frac{1}{2}(x - \bar{x})^* C^{-1}(x - \bar{x})\right] \tag{1}$$

From this it can be shown[1] that the probability that x is contained within the k-sigma hyperellipsoid

$$(x - \bar{x})^* C^{-1}(x - \bar{x}) = k^2 \tag{2}$$

is given by

$$p_n(k) = \operatorname{erf}[k/(2^{1/2})] - (2/\pi)^{1/2} \times \exp(-k^2/2)\left[k + \frac{k^3}{1\cdot 3} + \cdots + \frac{k^{n-2}}{1\cdot 3\cdot 5\cdots(n-2)}\right] \tag{3}$$

for odd n

$$p_n(k) = 1 - \exp(-k^2/2)\left[1 + \frac{k^2}{1\cdot 2} + \frac{k^4}{1\cdot 2\cdot 4} + \cdots + \frac{k^{n-2}}{1\cdot 2\cdot 4\cdots(n-2)}\right] \tag{4}$$

for even n

A graph of $p_n(k)$ vs k for selected values of n is given in Fig. 1.

When k is equal to 1 the very common "one-sigma" family of contours is encountered. It should be clear from Eqs. (3) and (4) that the probability that the random n-vector lies within the boundaries of these contours depends on n, i.e., it is $p_n(1)$ *not* $p_1(1)$ (68%) as is often incorrectly assumed. Specifically, $p_1(1)$ is the probability that any one element of the random vector lies between the intercepts of the hyperellipsoid with the corresponding coordinate axis *without* regard to where the remaining elements lie. In short, for $n > 1$, $p_n(1)$ assumes simultaneity, while $p_1(1)$ does not! Indeed, $p_n(1)$ is always smaller than $p_1(1)$ (see Fig. 1).

Another common misconception is that the square roots of the diagonal elements of the covariance matrix represent the lengths of the semiaxes of the one-sigma error hyperellipsoid. Actually, they bear no direct relationship to this contour. Note that the intercepts of the one-sigma hyperellipsoid with the coordinate axes are given by the reciprocal square roots of the diagonal elements of the *inverse* of the covariance matrix. These quantities, however, only provide an indication of the n-dimensional one-sigma error bounds and *do not*, in general, define the limits of this region. Only when the coordinate axes coincide with the principal axes does this distinction disappear.

Received August 28, 1970; revision received November 16, 1970.

* Staff Engineer, Satellite Navigation Department.

† Member Technical Staff, Satellite Navigation Department. Member AIAA.

Since the probability level corresponding to a one-sigma hyperellipsoid in n-space varies with n and is small for large n, it is generally more desirable to consider hyperellipsoids related to a specific probability confidence level (such as 50%). The analog of the covariance matrix for such a region can be found by multiplying the covariance matrix by the k^2 corresponding to any given $p_n(k)$. The resulting matrix can be conveniently named the "k-variance matrix," and the associated error contour called the "k-sigma hyperellipsoid." As with the covariance matrix, the square roots of the reciprocals of the diagonal elements of the inverse of the k-variance matrix represent the intercepts of this hyperellipsoid with the coordinate axes.

It is evident in many cases that the diagonal elements of the inverse of the covariance (or k-variance) matrix will not adequately describe the probability distribution of a given random vector. Now, in general, a hyperellipsoid in n-space is not very useful since it cannot be readily visualized. In addition, the enclosed region is meaningless if the various components of the random vector do not represent the same physical quantities (i.e., if they are not measured in commensurate units).

In such situations, insight can be gleaned by projection into lower dimensional subspaces, usually two- or three-space, in which each of the components can be expressed in the same units. Two possibilities are available: 1) two- or three-dimensional projections of a general n-dimensional hyperellipsoid which constrains all random variables can be considered; 2) k-sigma ellipses or ellipsoids can be found for compatible two-or three-element sets of the random vector *without regard* to the behavior of the remaining elements. In the former case, the desired contour is established by extracting the proper partition of the inverse of the k-variance matrix. In the latter case the desired ellipse or ellipsoid can be obtained by partitioning the covariance matrix first, multiplying the result by the appropriate k^2 for $p_2(k)$ or $p_3(k)$, and then performing a matrix inverse. In either case, the magnitudes and directions of the principal axes of the final contours can be found by solving the related eigenvalue-eigenvector problem.

Instead of considering the geometrical problems of displaying hyperellipsoid error regions, a possible alternative is to present results in terms of hyperspheres with the same probability level. Although this approach may seem appealing at first, it has accompanying disadvantages. Unless the principal axes of the given hyperellipsoid are nearly equal, use of the corresponding hypersphere can lead to serious errors in engineering judgment because all information regarding preferred directions will be lost. Furthermore, even when the use of hyperspheres is justifiable, the desired radius is not easily determined. For $n = 2$ and $n = 3$ special algorithms exist for this computation.[2,3] In these cases, when $p_n(k) =$

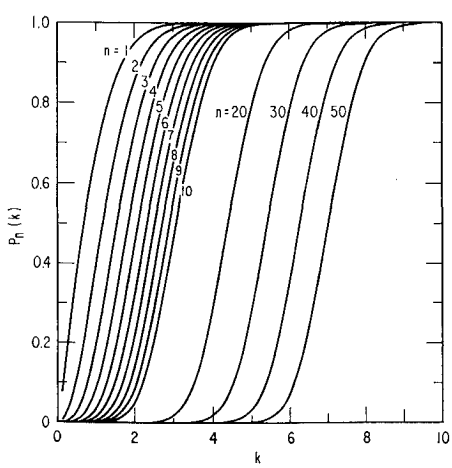

Fig. 1 $p_n(k)$ vs k for selected n.

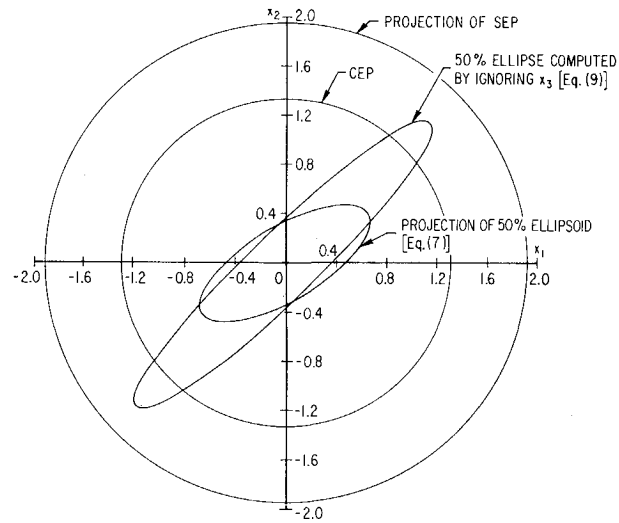

Fig. 2 Probability contours for example.

0.50, the results are the well-known circular error probability (CEP) and spherical error probability (SEP), respectively.

In order to understand the aforementioned concepts, consider the various 50% probability contours in the $x_1 - x_2$ plane associated with a zero-mean Gaussian random vector $x = (x_1,x_2,x_3)^*$ whose covariance matrix is

$$C = \begin{bmatrix} 1 & 0.95 & 0.90 \\ 0.95 & 1 & 0.95 \\ 0.90 & 0.95 & 1 \end{bmatrix} \tag{5}$$

First establish the $x_1 - x_2$ projection of the three-dimensional ellipsoid which encloses 50% of the values of x_1. As indicated previously, the appropriate partition of the inverse of the k-variance matrix must be found. For the case at hand, $n = 3$, $p_3(k) = 0.50$, so that Eq. (3) yields $k = 1.5382$. Thus one finds

$$(k^2C)^{-1} = \begin{bmatrix} 4.338 & -4.226 & 0.1122 \\ -4.226 & 8.453 & -4.226 \\ 0.1122 & -4.226 & 4.338 \end{bmatrix} \tag{6}$$

and the desired contour is given by the equation

$$[x_1x_2]\begin{bmatrix} 4.338 & -4.226 \\ -4.226 & 8.453 \end{bmatrix}\begin{bmatrix} x_1 \\ x_2 \end{bmatrix} = 1 \tag{7}$$

This result implicitly carries a constraint on x_3. As an alternative, a 50% contour in the $x_1 - x_2$ plane which imposes no constraint upon x_3 can be established. To accomplish this, first partition the C-matrix, then multiply by the k^2 satisfying $p_2(k) = 0.50$ [where from Eq. (4), $k = 1.1774$], and finally invert the result. The desired contour is thus given by

$$[x_1x_2]\left\{(1.1774)^2\begin{bmatrix} 1 & 0.95 \\ 0.95 & 1 \end{bmatrix}\right\}^{-1}\begin{bmatrix} x_1 \\ x_2 \end{bmatrix} = 1 \tag{8}$$

$$[x_1x_2]\begin{bmatrix} 7.399 & -7.029 \\ -7.029 & 7.399 \end{bmatrix}\begin{bmatrix} x_1 \\ x_2 \end{bmatrix} = 1 \tag{9}$$

Observe that the reciprocal square roots of the diagonal elements of the matrices in Eqs. (7) and (9) give the coordinate axes intercepts of the respective ellipses, while the solutions to the corresponding eigenvalue-eigenvector problem yield the principal axes and orientation angles. Note also that the square roots of the diagonal elements of the C-matrix are the standard deviations of the individual elements x_1, x_2, and x_3. Multiplying each by $k = 0.67449$ [obtained from Eq. (3) for $p_1(k) = 0.50$] gives the 50% boundaries on each element of x without regard to the behavior of the remaining two elements.

The various contours and boundaries discussed previously are illustrated in Fig. 2. For completeness, the CEP and the projection of the SEP are also shown on the diagram. The example shows the considerable variation possible for different contours associated with the same covariance matrix. The analyst, therefore, must carefully consider the alternatives and their interpretations before making a choice. While in general, there is no "best" geometric interpretation of a Gaussian probability distribution, error ellipses and ellipsoids are usually preferable since they contain more information than the other forms.

References

[1] Gura, I. A. and Gersten, R. H., "On Analysis of n-Dimensional Normal Probabilities," TR-0066(5129-01)-2, June 2, 1970, Aerospace Corp., El Segundo, Calif.

[2] Greenwalt, C. R. and Shultz, M. E., "Principles of Error Theory and Cartographic Applications," Rept. 96, Feb. 1962, Aeronautical Chart and Information Center, St. Louis, Mo.

[3] Schulte, R. J., "Four Methods of Solving the Spherical Error Probable Associated with a Three-Dimensional Normal Distribution," AD 666646, Jan. 1968, Holloman Air Force Base, N. Mex.

Effects of Prestress on Vibration Behavior of Certain Shells of Revolution

ALAN M. EBNER*
Drexel University, Philadelphia, Pa.

Nomenclature

E = modulus of elasticity
h = shell thickness
n = circumferential wave number
p = external pressure
p_0 = reference buckling pressure = $[2Eh^2/R^2][3(1-\nu^2)]^{-1/2}$
R = spherical shell radius
α = half opening angle of shell
λ = shallowness parameter = $[12(1-\nu^2)]^{1/4}[R\alpha^2/h]^{1/2}$
ν = Poisson's ratio
ρ = mass density
Ω = natural frequency
Ω_0 = reference frequency = $[E/\rho R^2(1-\nu^2)]^{1/2}$

Introduction

THE vibration and buckling behavior of shells of revolution have been studied extensively and numerous publications exist in the literature (see Refs. 1–6). However, data are lacking on the vibration behavior of prestressed shells which span the range between unstressed and buckled shells. These data are needed to provide a better understanding of the influence of prestress on vibration behavior and to provide results to which new analyses may be compared as they are developed. This Note presents the results of the vibration analysis of two prestressed shells of revolution obtained with the VALORS and BALORS programs which were early vibration and buckling versions of the SALORS (Stress Analysis of Layered Orthotropic Ring—Stiffened Shells of Revolution) System described in Ref. 7.

Shallow Spherical Cap

The clamped aluminum shallow spherical cap shown in Fig. 1 has a radius of 100 in., a half-opening angle of 20°, and a thickness of 1.094 in.; Young's modulus is 10^7 psi, and Poisson's ratio is $\frac{1}{3}$. The shallow shell parameter λ is 6. The shell is subjected to a uniform external pressure. The first-mode vibration behavior, for $n = 0$–4, was studied under the action of both linear and nonlinear prestress including prestress rotation. Initially the first natural frequencies of the unstressed shell were determined; resulting values of the frequency parameter Ω/Ω_0 are 1.4984, 1.1730, 1.3425, 1.6522, and 2.0629 for $n = 0, 1, \ldots, 4$, respectively, which compare favorably with frequencies for a similar shell in Ref. 8.

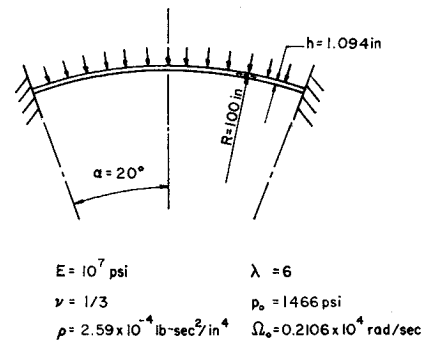

Fig. 1 Shallow spherical cap.

Figure 2 shows fundamental frequency vs prestress for several values of n and for both the linear and nonlinear prestress solutions. The pressures corresponding to zero frequency for the nonlinear prestress results agree with the buckling loads given by Huang;[9] those for the linear prestress agree with buckling loads obtained with the BALORS program and results given in Ref. 4. The results show the strong influence of the prestress nonlinearity on the frequencies of the shell as the load nears the buckling loads.

Conical Sandwich Shell

Figure 3 shows the conical sandwich shell. Properties are indicated clamped at the small end, free at the ring-stiffened large end, and subjected to an external uniform pressure. The shell is covered by a heat shield with substantial mass but negligible stiffness. A stress analysis and some of the

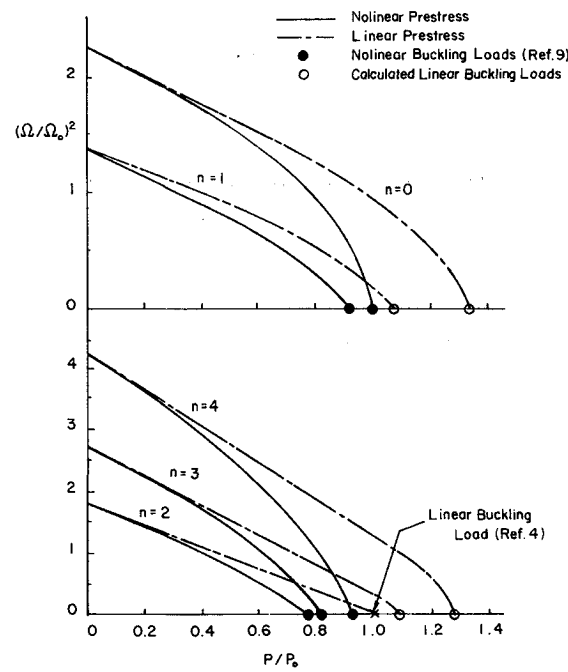

Fig. 2 Variation of natural frequencies of spherical cap with linear and nonlinear prestress (n = 0, 1, and 2,3,4).

Received August 18, 1970; revision received January 8, 1971. The author wishes to acknowledge the guidance of R. E. Fulton, of the NASA-Langley Research Center, who suggested this project while the author was a participant in the NASA-ASEE Summer Faculty Fellowship Program.

* Assistant Professor, College of Engineering.